Noninvasive Visualization of in Vivo Drug Delivery of Poly(l -glutamic acid) Using Contrast-Enhanced MRI

ARTICLE *in* MOLECULAR PHARMACEUTICS · OCTOBER 2006

Impact Factor: 4.38 · DOI: 10.1021/mp060052g · Source: PubMed

7 AUTHORS, INCLUDING:

Eun-Kee Jeong
University of Utah
121 PUBLICATIONS **2,552** CITATIONS
SEE PROFILE

Zheng-Rong Lu
Case Western Reserve University
123 PUBLICATIONS **3,389** CITATIONS
SEE PROFILE

Published in final edited form as:
Mol Pharm. 2006 ; 3(5): 507–515.

Non-invasive visualization of in vivo drug delivery of poly(*L*-glutamic acid) using contrast enhanced MRI

Furong Ye[1], **Tianyi Ke**[1], **Eun-Kee Jeong**[2], **Xuli Wang**[1], **Yongen Sun**[1], **Melody Johnson**[2], and **Zheng-Rong Lu**[1,*]

1*Department of Pharmaceutics and Pharmaceutical Chemistry, University of Utah, Salt Lake City, Utah 84108*

2*Department of Radiology, University of Utah, Salt Lake City, Utah 84108*

Abstract

Biomedical imaging is valuable for non-invasive investigation of *in vivo* drug delivery with polymer conjugates. It can provide real-time information on pharmacokinetics, biodistribution and drug delivery efficiency of the conjugates. Non-invasive visualization of in vivo drug delivery of polymer conjugates with contrast enhanced magnetic resonance imaging (MRI) was studied with paramagnetically labeled poly(*L*-glutamic acid) in an animal tumor model. Poly(*L*-glutamic acid) is a biocompatible and biodegradable drug carrier for diagnostics and therapeutics. Poly(*L*-glutamic acid)-1,6-hexanediamine-(Gd-DO3A) conjugates with molecular weights of 87, 50 and 28 KDa and narrow molecular weight distributions were prepared and studied in mice bearing MDA-MB-231 human breast cancer xenografts. Contrast enhanced MRI resulted in real-time and three-dimensional visualization of blood circulation, pharmacokinetics, biodistribution and tumor accumulation of the conjugates, and the size effect on these pharmaceutics properties. The conjugate of 28 KDa rapidly cleared from the circulation and had a relatively lower tumor accumulation. The conjugates with higher molecular weights exhibited a more prolonged blood circulation and higher tumor accumulation. The difference between the conjugates of 87 and 50 KDa was not significant. Contrast enhanced MRI is effective for non-invasive real-time visualization of *in vivo* drug delivery of paramagnetically labeled polymer conjugates.

Introduction

Biocompatible polymer conjugates are effective drug delivery systems for diagnostics and therapeutics [1-4]. Water-soluble biomedical polymers have a prolonged blood circulation time and the conjugation of diagnostics and therapeutics to the polymers significantly modify their pharmacokinetics and pharmacodynamics. The conjugation of anticancer drugs to water-soluble polymers increases their bioavailability, prolongs in vivo drug retention time, reduces systemic toxicity and enhances therapeutic efficacy of the drugs [5-7]. Polymer-drug conjugates can passively accumulate within solid tumor tissues due to the hyperpermeability of tumor blood vessels and poor lymphatic drainage of tumor tissues, a phenomenon termed as “enhanced permeability and retention (EPR) effect” [8]. They also have a potential to overcome multiple drug resistance [9]. Currently, several polymer drug conjugates are available in clinical cancer treatment, and more are in the pipeline of clinical development.

*Correspondence: Zheng-Rong Lu, PhD Department of Pharmaceutics and Pharmaceutical Chemistry University of Utah 421 Wakara Way, Suite 318 Salt Lake City, UT 84108 Tel: (801) 587−9450 Fax: (801) 585−3614 Email: ZhengRong.Lu@utah.edu.

Although significant progress has been made in the development of polymeric conjugates, the understanding of *in vivo* drug delivery mechanisms, including interactions of the polymers with tissues and organs, the influence of polymer structure on drug delivery efficiency, process of *in vivo* transport, and the correlation of delivery efficiency with therapeutic efficacy, is insufficient due to the limitations of currently available methods used in both pre-clinical and clinical studies. *In vitro* tests at the cellular level cannot provide adequate information for prediction of the *in vivo* behavior of the conjugates. Subtle changes in the physiological environment often complicate the therapeutic outcome of the drug delivery systems [10,11]. Traditional *in vivo* evaluation of polymer-drug conjugates are based on blood and urine sampling, or surgery and symptom-based observations. These methods cannot accurately provide real-time information about the *in vivo* behavior of polymer conjugates. A large number of animals are also required in the studies. More importantly, these methods cannot be effectively applied for evaluating drug delivery in humans. Consequently, the data obtained by conventional methods in the preclinical studies cannot be used to accurately predict clinical outcome in human. Therefore, appropriate approaches are needed to understand the *in vivo* drug delivery of polymer conjugates at both molecular and macroscopic levels. More accurate understanding of in vivo drug delivery with polymer conjugates would be valuable for the design and development of more efficiency and efficacious drug delivery systems.

Recent advances in biomedical imaging have provided the essential tools for non-invasive and real-time *in vivo* evaluation for drug delivery [12-15]. Noninvasive imaging assessment will be more effective in determination of the pharmacokinetics, biodistribution, target deposition and drug delivery efficiency of polymer drug conjugates. Several imaging modalities including gamma scintigraphy, single photon emission computed tomography (SPECT), positron emission tomography (PET), computed tomography (CT) and magnetic resonance imaging (MRI) are available for clinical studies in human subjects. Nuclear medicine has high sensitivity, but has a poor spatial resolution for anatomic analysis. Computed tomography can produce good spatial resolution, but a much higher dose of contrast agent is required. MRI is a non-invasive imaging modality and provides three-dimensional images of anatomic structures with high spatial resolution [16-18]. Paramagnetic chelates (e.g. Gd(III) chelates) are often used as MRI contrast agents to enhance the signal in target tissue for accurate diagnosis. Contrast enhanced MRI would be a useful approach for non-invasive visualization of *in vivo* drug delivery of polymer conjugates.

In this study, we explored a non-invasive method for evaluating in vivo drug delivery of polymer conjugates with contrast enhanced MRI in a mouse tumor model with paramagnetically labeled poly(*L*-glutamic acid) (PGA) of different sizes as model conjugates. Poly(*L*-glutamic acid) is a biocompatible and biodegradable polymeric drug carrier. Several poly(*L*-glutamic acid) anticancer drug conjugates have been developed and some of them are now in various stages of clinical trials [19-21]. Poly(*L*-glutamic acid) was labeled with stable paramagnetic chelate Gd-DO3A (1,4,7,10-tetraazacyclododecane-1,4,7-trisacetic acid) and fractionated into different molecular weights with a narrow molecular weight distribution. The conjugates with molecular weights of 87 KDa, 50 KDa and 28 KDa were selected to study non-invasive visualization of *in vivo* drug delivery. Non-invasive dynamic contrast-enhanced MRI clearly revealed the size effect of the conjugates on their pharmacokinetics, biodistribution and tumor accumulation.

Experimental Section

Materials

Bromoacetic acid, 1,6-hexanediamine, N-hydroxysuccinimide (NHS) and N-diisopropylethylamine (DIEA) were purchased from Lancaster Synthesis, Inc (Pelham, NH). 1,4,7,10-Tetraazacyclododecane (cyclen) was purchased from Macrocyclics (Dallas, TX). Di-

tert-butyl dicarbonate was purchased from Nova Chemicals (La Jolla, CA). Gadolinium(III) acetate and *tert*-butyl bromoacetate were purchased from Alfa Aesar (Ward Hill, MA). 1-Ethyl-3-(3-dimethylaminopropyl)carbodiimide HCl (EDC) was purchased from Pierce (Rockford, IL). Optima nitric acid was purchased from Fisher Chemical (Pittsburgh, PA). The MDA-MB-231 human breast cancer cell line, Leibovitz's L-15 medium with 2 mM *L*-glutamine, and 10% FBS were purchased from the American Type Culture Collection (ATCC, Manassas, VA). Poly(*L*-glutamic acid) (M_w = 90 KDa, M_n = 63 KDa) was synthesized according to a literature method [22]. Poly(*L*-glutamic acid) N-hydroxysuccinimide active ester (PGA-OSu) was synthesized according to a reference method [23]. Mono-N-*t*-Boc-1,6-hexanediamine was prepared according to a literature method [24]. 1,4,7,10-Tetraazacyclododecane-1,4,7-triacetic acid (DO3A) was synthesized according to a literature method [25].

Synthesis of 1,4,7,10-tetraazacyclododecane-1,4,7-tri(acetic acid)-10-(acetic acid-1,6-hexanediamine monoamide)

DO3A-N-Boc-1,6-diaminohexane monoamide was synthesized by the reaction of DO3A (0.7 g, 2 mmol) with the N-Boc-1,6-diaminohexane bromoacetamide (0.67 g, 2 mmol) in a mixture of methanol and triethylamine (20 ml, 2:1) and excess K_2CO_3 (2.76 g). The reaction was carried out for 24 hours at room temperature. The inorganic precipitate was filtered off and the solvent was evaporated under vacuum. The residue was washed with ether, followed by acetone, and dried under vacuum. The N-Boc protection was removed by dissolving the residue in a minimum amount of cold trifluoroacetic acid for 15 minutes. DO3A-AHM was finally precipitated in either and dried under vacuum. Yield: 0.8 g, 80%. ^{1}HNMR, δ_H (D_2O, ppm): 3.38−3.90 (8H, m, CH_2CO), 2.75−3.30 (20H, m, -CH_2N- of the ring and NCH_2 of 1,6-hexanediamine), 1.06−1.51 (8H, m, $(CH_2)_4$). ESI-MS (m/z, $M+H^+$): 503.5 (measured), 503.3 (calculated).

Synthesis of PGA-1,6-hexanediamine-(Gd-DO3A) conjugate

PGA-OSu (100 mg) and 4-dimethylaminopyridine (360 mg, 2.95 mmol) was dissolved in 12 ml anhydrous DMF. 1,4,7,10-Tetraazacyclododecane-1,4,7-tris(acetic acid)-10-(acetic acid-1,6-hexanediamine monoamide) (483.4 mg, 0.44 mmol) was then added to above mixture. The reaction mixture was stirred overnight at room temperature and the product was precipitated from acetone. The final product was prepared by the complexation of PGA-1,6-hexanediamine-DO3A conjugate with an excess of $Gd(OAc)_3$ (200 mg) in deionized water at pH 5−6. Xylenol Orange indicator was added into the solution and EDTA was then added until the pink color disappeared. The polymer conjugate was purified by dialysis with Spectra/Por® 6 membrane (molecular weight cut-off: 25,000) against deionized water.

PGA-1,6-hexanediamine-(Gd-DO3A) conjugate was fractionated using with a 16/60 Superdex 200 prep grade column to prepare the conjugate with different molecular weights and narrow molecular weight distributions. Polymer conjugate was loaded into the column at a concentration of 25 mg/ml and eluted with TRIS buffer. The fractions were collected and purified using a PD-10 desalting column. The polymer conjugate fractions were obtained after lyophilization and their molecular weights were determined by size exclusion chromatography (SEC) with an AKTA FPLC system, calibrated with standard poly[N-(2-hydroxypropyl) methacrylamide]. Gd(III) content of the conjugate was determined by inductively coupled plasma-optical emission spectroscopy (ICP-OES) (Perkin-Elmer, Norwalk, CT, Optima 3100XL) at 342nm.

T_1 relaxivity measurement

T_1 relaxivity of the PGA-(Gd-DO3A) conjugates was measured by a standard inversion recovery sequence on a Siemens Trio 3T MRI scanner. Three concentrations of each sample

were placed in a RF coil and scanned at 10 different inversion times (TI) from 200 to 2500 ms. Signal intensities in the regions of interest (ROI) were calculated and T_1 relaxation times were analyzed by non-linear regression fitting of the signal enhancement data, using equation $M_{TI} = M_0(1-2e^{(-TI/T1)})$, where M_{TI} is the net amplitude of a selected ROI at time TI, and M_0 is the maximum amplitude that are acquired from the equilibrium longitudinal magnetization. Relaxivity was calculated from the slope of the plot of $1/T_1$ versus the concentrations [26].

MR Imaging

The polymer conjugates were evaluated in female athymic nude mice (22−25 g, Charles River Laboratories) bearing MDA-MB-231 human breast carcinoma xenografts. The animals were cared for under the guidelines of University of Utah Institutional Animal Care and Use Committee. The tumor model was developed with the same protocol as previously reported [27]. Imaging experiment was carried out when the tumor size reached 0.8−1.0 cm in diameter. The mice were anesthetized by intramuscular administration of a mixture of ketamine (45 mg/kg) and xylazine (6 mg/kg). The polymer conjugates were injected at a dose of 0.03 mmol-Gd/kg into the anesthetized mice via a tail vein. The conjugates with each molecular weight were studied in a group of three mice. Contrast-enhanced images were acquired before and after injection on a Siemens Trio 3T MRI scanner with a wrist coil. A 3D FLASH pulse sequence were used with 1.74 ms echo time (TE), 4.3 ms repetition time (TR), 25° RF tip angle, 120 mm field of view (FOV), and spatial resolution of 0.4_0.4_0.5 mm^3. MR images were acquired continuously for the first 20 minutes and then at 30, 60, 120, 180, 240, 360, and 1440 minutes (24 hour) post-injection. MR images were analyzed with Osirix (http://homepage.mac.com/rossetantoine/osirix/) software. In each animal, the ROIs were set on heart, kidney, liver and tumor tissues. Signal intensity in similar ROIs was determined from the source images for each animal at various time points. Relative signal intensities in the major organs and tumor tissues were calculated as the ratios of the signal intensities after injection to that of pre-injection. The profiles of the signal intensities of pixels along a line within the tumor tissues were analyzed with ImageJ software (http://rsb.info.nih.gov/ij/). Similar cross-section positions were selected for each animal. Three dimensional plots of signal intensities along the line at various time points were plotted to evaluate the dynamic changes of the polymer conjugates cross solid tumors.

Statistical analysis was performed with Prism software (Version 4.0b, GraphPad software Inc., San Diego, CA) using two-way repeated ANOVA. Bonferroni post-test was used to determine the difference significance in the comparisons among the conjugates. Statistical significance was considered when $p < 0.05$.

RESULTS

The synthetic procedure of poly(*L*-glutamic acid)-1,6-hexanediamine-(Gd-DO3A) is described in Scheme 1. The polymer conjugate had a broad molecular weight distribution. The conjugate was fractionated by size exclusion chromatography to prepare conjugates with different molecular weights and narrow molecular weight distributions. Table 1 lists the collected fractions and their physicochemical properties including average molecular weights, Gd contents and T_1 relaxivity. All fractions except for fractions 1 and 2 had a narrow molecular weight distribution with $M_w/M_n < 1.1$. High polydispersity of fractions 1 and 2 was due to the limitation of the preparative column in separation of the high molecular weight polymers. The Gd content varied in the range of 30 − 55 mol-% among the fractions. Fractions 1, 4 and 8 with weight average molecular weight of 87, 50 and 28 KDa were selected to represent polymer conjugates with high, intermediate and low molecular weights for study of *in vivo* drug delivery.

T_1 relaxivity of the polymer conjugates was in the range of 9.2 − 10.6 $mM^{-1}s^{-1}$ per conjugate Gd(III) chelate at 3 Tesla. It appears that the molecular weight of conjugates did not significantly affect their relaxivity. The fractions selected for *in vivo* study had similar T_1 relaxivity, which was 9.45, 9.44 and 9.19 $mM^{-1}s^{-1}$ for the high, intermediate and low molecular weight conjugates, respectively.

Three-dimensional MR mouse images were acquired before and at various time points after the injection of the conjugates. Figure 2 shows representative T_1-weighted coronal image slices of mice crossing the heart, liver and tumor tissue with the conjugates of three different molecular weights. The MR images clearly revealed the distribution of the conjugates in the blood, major organs and tumor tissue at different time points and molecular weight dependent circulation of the conjugates in the body. The signal intensity indirectly reflects the concentration of the conjugates in the organs or tissues. Bright signal indicates high concentrations of the conjugates. High signal intensities in the abdomen resulted from the intrinsic signal from the stomach and intestines. Strong contrast enhancement was observed in the liver and blood in the heart through the first minute post-injection for all conjugates. The signal gradually faded away depending on the size of the conjugates. The signal for the conjugate of 28 KDa disappeared much faster than the conjugates of higher molecular weights, indicating rapid clearance of the low molecular weight conjugate. At 60 minutes post-injection, the enhancement in the blood for the low molecular weight conjugate returned to the background level. The molecular weight conjugate of 87 KDa had the longest circulation among the conjugates and significant enhancement was still observed at 24 hours post-injection. No significant contrast enhancement was observed in the lung for the conjugates.

The change of the relative signal intensities in the blood and liver up to 24 hours is shown in Figure 2. Since the conjugates with different molecular weights had similar T_1 relaxivity, the signal ratios should reflect the relative concentration of the conjugates in the blood and liver, and time course of the signal ratios should correlate to the pharmacokinetics of the conjugates. The quantitative analysis of signal intensity showed that blood circulation of the conjugates of molecular weights of 87 KDa and 50 KDa was similar up to 6 hours post-injection ($p > 0.05$) and the blood retention of the conjugate of molecular weight 28 KDa was significantly lower than that of the conjugate of 87 KDa and 50 KDa ($p < 0.05$ for both). The conjugate of 28 KDa cleared rapidly from the blood within 1 hour. The size of the polymer conjugates had a significant impact on their blood pharmacokinetics. The kinetics of signal intensity of the conjugates in the liver had a similar size-dependent pattern as those in the blood except that the clearance of the conjugates from the liver was slow. High signal intensities were still observed for all conjugates in the liver at 24 hours post-injection, indicating high liver accumulation of the conjugates.

The size of the conjugates also had a significant impact on tumor signal enhancement although the enhancement was not as strong as in the blood and liver. Stronger enhancement was observed in the tumor periphery than tumor interstitium, Figure 1. Figure 3 shows the dynamic changes of the relative signal intensities of the tumor periphery and interstitium at various time points post-injection as compared to those before injection. Polymer conjugates with high molecular weights (87 and 50 KDa) resulted in more prolonged enhancement in both tumor periphery and interstitium than the low molecular weight conjugate. The difference between the conjugates with molecular weights of 50 and 87 KDa was not significant. Figure 4 shows the representative dynamic changes of signal intensity distribution of the conjugates cross the tumor tissues. It shows the distribution of the conjugates in the tumor tissue and change of the distribution. It can be clearly seen that the distribution of the conjugates in the tumor was heterogeneous and dynamic. The size of the conjugates significantly affected their distribution and retention in the tumor tissue. Accumulation of the conjugates with high molecular weights

gradually increased across tumor and maintained for a prolonged period. The conjugate with 28 KDa had a relatively low distribution and cleared rapidly from the tissue.

DISCUSSION

Contrast enhanced MRI allows non-invasive visualization of real-time pharmacokinetics and biodistribution of the paramagnetically labeled polymer conjugates with high spatial resolution. Although MR signal intensity is not linearly correlated to the concentration of the Gd(III) chelates in the conjugates, it provides qualitative and semi-quantitative information of real-time in vivo biodistribution of the polymeric conjugates. As compared to the conventional surgery-based pharmacokinetic studies, the observations with MRI are made continuously in the same group of experimental animals and the number of animals used is greatly reduced in the study. Dynamic changes of heterogeneous distribution of the conjugates in the tumor tissues were clearly revealed in the MR images, which could be a critical factor for the therapeutic efficacy of polymer anticancer drug conjugates. In comparison, the conventional pharmacokinetic study only provides the average drug concentration in the target tissues.

In this study, contrast enhanced MRI also clearly revealed the size effect of the conjugates on the blood pharmacokinetics, distribution in major organs and tumor tissues as a function of time. Polymeric conjugates with high molecular weights had a prolonged blood circulation and higher tumor accumulation than low molecular weight conjugate, which is consistent to the results obtained with conventional pharmacokinetic studies [28,29]. The conjugate with 28 KDa eliminated rapidly from both blood pool and major organs due to its small size and fast excretion through renal filtration and had a relatively low tumor accumulation with short duration time. The renal filtration threshold could be the dominant factor on the size effect of the conjugates. The conjugates with high molecular weights had sizes larger than the renal filtration threshold and consequently a prolonged *in vivo* retention. Since poly(*L*-glutamic acid) is biodegradable, the conjugates with high molecular weights underwent degradation and gradually excreted from the body as shown in the dynamic MR images.

Analysis of signal intensities also indicates that the conjugates with high molecular weights resulted in longer blood circulation and more prominent accumulation across tumor tissue. This suggests that drug delivery with polymer conjugates into tumor tissues is a gradual process and polymer conjugates with high molecular weights and long blood circulation are more efficient drug delivery systems than the low molecular weight conjugates. Consequently, polymer conjugates with high molecular weights may have higher therapeutic efficacy.

In vivo drug delivery with polymer conjugates have also been investigated non-invasively in animal models with γ-scintigraphy [30,31]. Scintigraphic imaging has a high sensitivity and provides more accurate quantitative information on in vivo biodistribution, but suffers poor spatial resolution. It is difficult to directly correlate the scintigraphic data to the anatomic structure of the body without assistant of other imaging modalities including CT and MRI [32]. In comparison, contrast enhanced MRI provides three-dimensional images of the biodistribution of the conjugates in the body with high spatial resolution. The accuracy of quantitative evaluation of *in vivo* drug delivery with polymeric conjugates can be improved with currently available quantitative MRI technology including T_1 mapping [33,34]. Quantitative T_1 measurement and mapping have a potential to accurately correlate the change in the apparent T_1 values of water protons in the tissue of interest to the concentration of paramagnetically labeled polymer conjugates. However, the quantitative technique may suffer from limited spatial resolution and image volume coverage, particularly to obtain improved temporal resolution. The combination of pseudo-T_1 weighted high-resolution 3D imaging and quantitative T_1 mapping will be a powerful tool for non-invasive evaluation of *in vivo* drug delivery with polymer conjugates. The accurate understanding of the mechanisms and

structural factors of the conjugates on *in vivo* drug delivery efficiency will be valuable for the design of more efficient drug delivery systems.

In summary, contrast enhanced MRI was effective for non-invasive evaluation of *in vivo* drug delivery of paramagnetically labeled polymer conjugates. The size effect of the conjugates on their pharmacokinetics, biodistribution and tumor targeting observed with MRI was consistent to the results obtained with conventional surgery-based methods. Contrast enhanced MRI is advantageous for non-invasive and continuous acquiring the real-time and three-dimensional information of *in vivo* drug delivery of the polymer conjugates with a small number of experimental animals.

Acknowledgments

This research was supported in part by NIH grant R01 CA097465. We thank Dr. Dennis Parker for valuable discussions on the research project.

References

1. Haag R, Kratz F. Polymer Therapeutics: Concepts and Applications. Angew. Chem. Int. Ed 2006;45:1198–1215.
2. Maeda H, Seymour LW, Miyamoto Y. Conjugates of Anticancer Agents and Polymers: Advantages of Macromolecular Therapeutics *in vivo*. Bioconjugate Chem 1992;3:351–362.
3. Kopecek J, Kopeckova P, Minko T, Lu Z-R. HPMA Copolymer-Anticancer Drug Conjugates: Design, Activity, and Mechanism of Action. Eur. J. Pharm. Biopharm 2000;50:61–81. [PubMed: 10840193]
4. Lu Z-R, Wang X, Parker DL, Goodrich KC, Buswell HR. Poly(*L*-glutamic acid) Gd(III)-DOTA Conjugate with a Degradable Spacer for Magnetic Resonance Imaging. Bioconjugate Chem 2003;14:715–719.
5. Benjamin RS. Pharmacokinetics of Adriamycin (NSC-123127) in Patients with Sarcomas. Cancer Chemother. Rep 1974;58:271–273. [PubMed: 4830501]
6. Newell DR. Pharmacokinetic Determinants of the Activity and Toxicity of Antitumour Agents. Cancer Surv 1989;8:557–603. [PubMed: 2701085]
7. Duncan R, Kopeckova P, Strohalm J, Hume I, Cable HC, Pohl J, Lloyd JB, Kopecek J. Anticancer Agents Coupled to *N*-(2-hydroxypropyl)methacrylamide copolymers. I. Evaluation of Daunomycin and Puromycin Conjugates *in vitro*. Br. J. Cancer 1987;55:165–174. [PubMed: 3468994]
8. Maeda H, Seymour LW, Miyamoto Y. Conjugates of Anticancer Agents and Polymers: Advantages of Macromolecular Therapeutics *in Vivo*. Bioconjugate Chem 1992;3:351–362.
9. Minko T, Kopeckova P, Kopecek J. Chronic Exposure to HPMA Copolymer-Bound Adriamycin Does Not Induce Multidrug Resistance in a Human Ovarian Carcinoma Cell Line. J. Control. Release 1999;59:133–148. [PubMed: 10332049]
10. Hobbs SK, Monsky WL, Yuan F, Roberts WG, Griffith L, Torchilin VP, Jain RK. Regulation of Transport Pathways in Tumor Vessels: Role of Tumor Type and Microenvironment. Proc. Natl. Acad. Sci. USA 1998;95:4607–4612. [PubMed: 9539785]
11. Jain RK. Transport Phenomena in Tumors. Adv. Chem. Eng 1994;19:129–200.
12. Newman SP, Wilding IR. Imaging Techniques for Assessing Drug Delivery in Man. Pharm. Sci. & Technol. Today 1999;2:181–189. [PubMed: 10322380]
13. Richardson JC, Bowtell RW, Mader K, Melia CD. Pharmaceutical Applications of Magnetic Resonance Imaging (MRI). Adv. Drug Deliv. Rev 2005;57:1191–1209. [PubMed: 15935869]
14. Wen X, Cao X, Pasuelo MJ, Wendt R, Li C. Polymeric Radiotracers in Nuclear Imaging. Curr. Drug Deliv 2004;1:377–384. [PubMed: 16305399]
15. Massoud TF, Gambhir SS. Molecular Imaging in Living Subjects: Seeing Fundamental Biological Processes in a New Light. Genes Dev 2003;17:545–580. [PubMed: 12629038]
16. Taylor JS, Reddick WE. Evolution from Empirical Dynamic Contrast-Enhanced Magnetic Resonance Imaging to Pharmacokinetic MRI. Adv. Drug Deliv. Rev 2000;41:91–110. [PubMed: 10699307]

17. Griffiths JR, Glickson JD. Monitoring Pharmacokinetics of Anticancer Drugs: Non-Invasive Investigation Using Magnetic Resonance Spectroscopy. Adv. Drug Deliv. Rev 2000;41:75–89. [PubMed: 10699306]
18. Stark, DD.; William, G, Jr.. Magnetic Resonance Imaging. The C.V. Mosby Company.; St. Louis, Missouri: 1988. Bradley..
19. Sabbatini P, Aghajanian C, Dizon D, Anderson S, Dupont J, Brown JV, Peters WA, Jacobs A, Mehdi A, Rivkin S, Eisenfeld AJ, Spriggs D. Phase II Study of CT-2103 in Patients With Recurrent Epithelial Ovarian, Fallopian Tube, or Primary Peritoneal Carcinoma. J. Clin. Oncol 2004;22:4523–4531. [PubMed: 15542803]
20. Auzenne E, Donato NJ, Li C, Leroux E, Price RE, Farquhar D, Klostergaard J. Superior Therapeutic Profile of Poly-L-Glutamic Acid-Paclitaxel Copolymer Compared with Taxol in Xenogeneic Compartmental Models of Human Ovarian Carcinoma. Clin. Cancer Res 2002;8:573–581. [PubMed: 11839679]
21. Bhatt R, Vries P, Tulinsky J, Bellamy G, Baker B, Singer JW, Klein P. Synthesis and in Vivo Antitumor Activity of Poly(L-glutamic acid) Conjugates of 20(S)-Camptothecin. J. Med. Chem 2003;46:190–193. [PubMed: 12502373]
22. Idelson M, Blout ER. Polypeptides. XXI. High Molecular-Weight Poly(_,*L*-glutamic acid): Preparation and Optical Rotation Changes. J. of the Amer. Chem. Soc 1958;80:4631–4634.
23. Iwata H, Matsuda S, Mitsuhashi K, Itoh E, Ikada YA. Novel Surgical Glue Composed of Gelatin and *N*-hydroxysuccinimide Activated Poly(L-glutamic acid): Part 1. Synthesis of Activated Poly(L-glutamic acid) and Its Gelation with gelatin. Biomaterials 1998;19:1869–1876. [PubMed: 9855188]
24. Callahan JF, Ashton-Shue D, Bryan HG, Bryan WM, Heckman GD, Kinter LB, McDonald JE, Moore ML, Schmidt DB, Silvestri JS, Stassen FL, Sulat L, Yim NCF, Huffman WF. Structure-Activity Relationships of Novel Vasopressin Antagonists Containing C-terminal Diaminoalkanes and (Aminoalkyl)guanidine. J. Med. Chem 1989;32:391–396. [PubMed: 2521519]
25. Beeby A, Bushby LM, Maffeo D, Willams JAG. Intramolecular Sensitization of Lanthanide(III) Luminescence by Acetophenone-Containing Ligands: the Critical Effect of Para-substituents and Solvent. J. Chem. Soc., Dalton Trans 2002;1:48–52.
26. Fukushima, E.; Roeder, SBW. Experimental Pulse NMR: a Nuts and Bolts Approach. Addison-Wesley; Reading, MA: 1981.
27. Yuda Z, Wang X, Goodrich KC, Mohs AM, Parker DL, Lu Z-R. Contrast-Enhanced MRI With New Biodegradable Macromolecular Gd(III) Complexes in Tumor-Bearing Mice. Mag. Reson. Med 2005;53:835–84.
28. Veronese FM, Schiavon O, Pasut G, Mendichi R, Andersson L, Tsirk A, Ford J, Wu G, Kneller S, Davies J, Duncan R. PEG-doxorubicin Conjugates: Influence of Polymer Structure on Drug Release, in Vitro Cytotoxicity, Biodistribution, and Antitumor Activity. Bioconjugate Chem 2005;16:775–784.
29. Seymour LW, Miyamoto Y, Maeda H, Brereton M, Strohalm J, Ulbrich K, Duncan R. Influence of Molecular Weight on Passive Tumour Accumulation of a Soluble Macromolecular Drug Carrier. Eur. J. Cancer 1995;31A:766–770. [PubMed: 7640051]
30. Kissel M, Peschke P, Subr V, Ulbrich K, Schuhmacher J, Debus J, Friedrich E. Synthetic Macromolecular Drug Carriers: Biodistribution of Poly[(*N*-2-hydroxypropyl)methacrylamide] Copolymers and Their Accumulation in Solid Rat Tumors. PDA J. of Pharmaceutical Sci. & Tech 2001;55:191–201.
31. Lammers T, Kuhnlein R, Kissel M, Subr V, Etrych T, Pola R, Pechar M, Ulbrich K, Storm G, Huber P, Peschke P. Effect of Physicochemical Modification on the Biodistribution and Tumor Accumulation of HPMA Copolymers. J. Control. Release 2005;110:103–118. [PubMed: 16274831]
32. Mitra A, Nan A, Hamidreza G, McNeill E, Mulholland J, Line BR. Technetium-99m-Labeled *N*-(2-hydroxypropyl) methacrylamide Copolymers: Synthesis, Characterization, and *in vivo* distribution. Pharm. Res 2004;21:1153–1159. [PubMed: 15290854]
33. Gohr-Rosental S, Schmitt-Willich H, Ebert W, Conrad J. The Demonstration of Human Tumors on Nude Mice Using Gadolinium-Labelled Monoclonal Antibodies for Magnetic Resonance Imaging. Invest. Radiol 1993;28:789–795. [PubMed: 8225882]

34. Liu X, Feng Y, Ke T, Lu Z-R, Li KS, Morrell G, Jeong E-K. Rapid Data Acquisition for T1 Mapping, Using Multishot EPI and Automated TR Variation at 3T. 2006ISMRM abstract

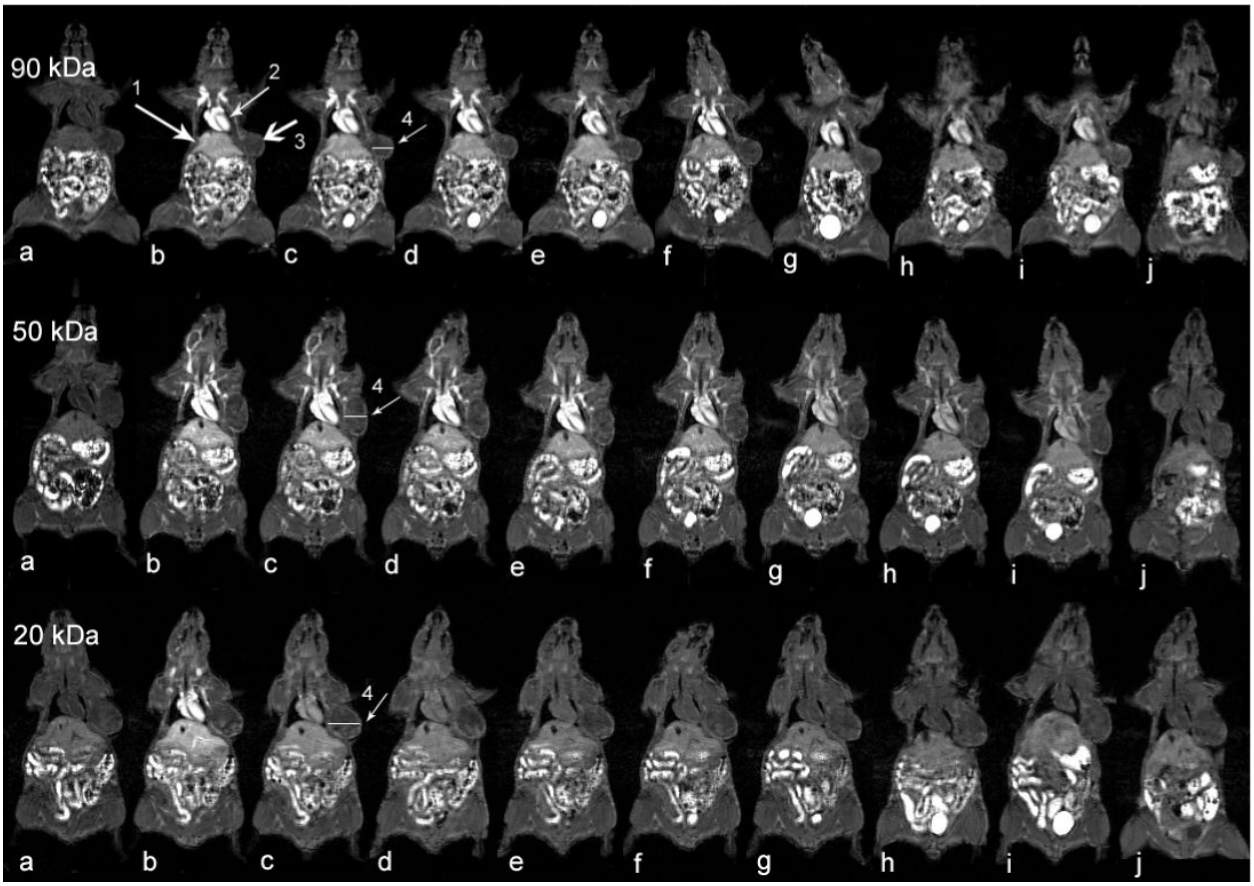

Figure 1.

Coronal MR images of tumor bearing mice before (a) and at 1 (b), 11 (c), 20 (d), 30 (e), 60 (f), 120 (g), 180 (h), 240 (i) minutes and 24 hours (j) after injection of PGA-1,6-hexanediamine-(Gd-DO3A) conjugates of different molecular weights. Arrows are pointing to the liver (1), heart (2), tumor tissue (3) and cross section is for plot profile analysis in Figure 4 (4).

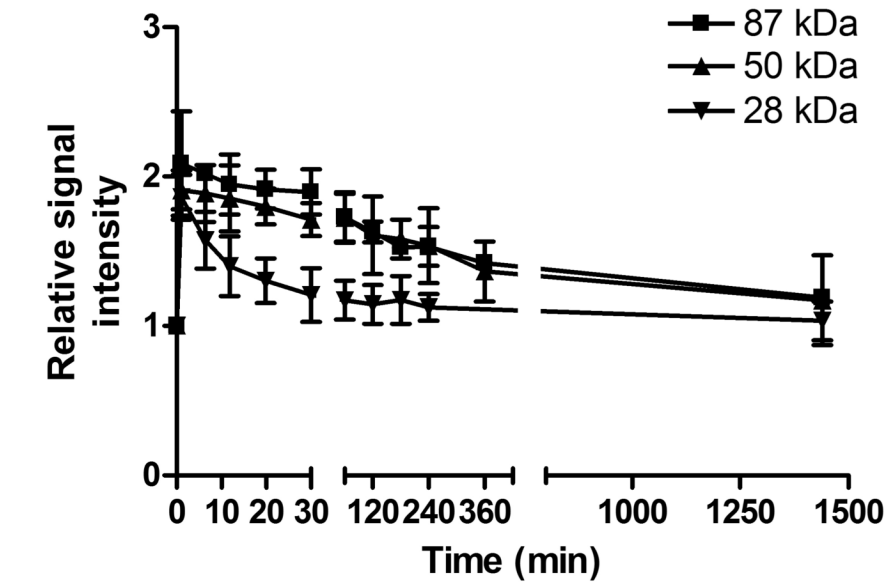

(A)

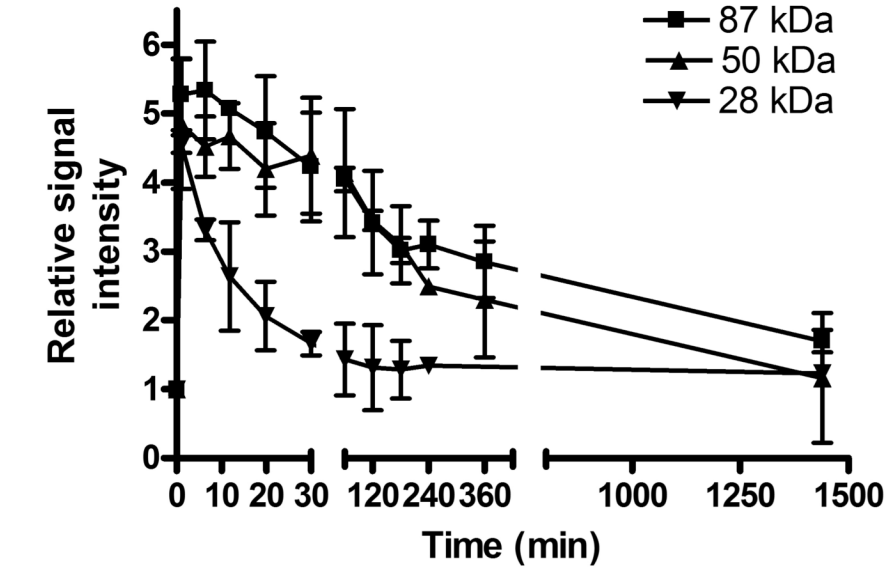

(B)

Figure 2.
Relative signal intensities in the blood (A) and liver (B) before and at various time points after the injection of PGA-1,6-hexanediamine-(Gd-DO3A) conjugates.

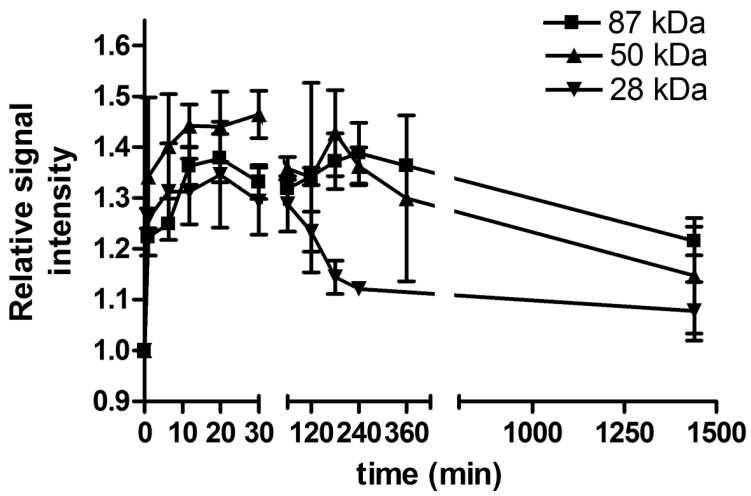

(3A)

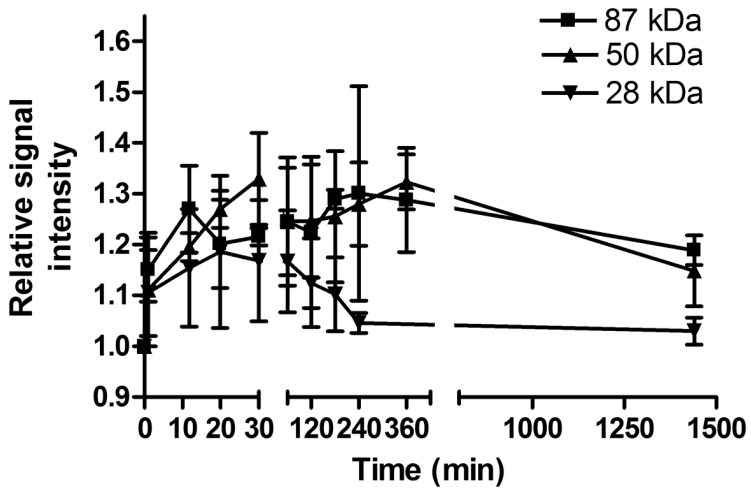

(3B)

Figure 3.
Relative signal intensities in tumor periphery (A) and interstitium (B) before and at various time points after the injection of PGA-1,6-hexanediamine-(Gd-DO3A) conjugates.

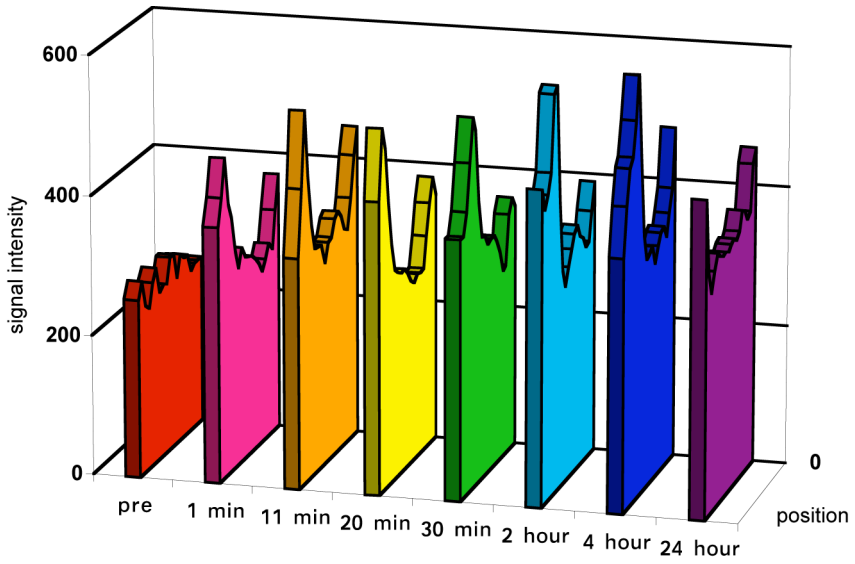

(A)

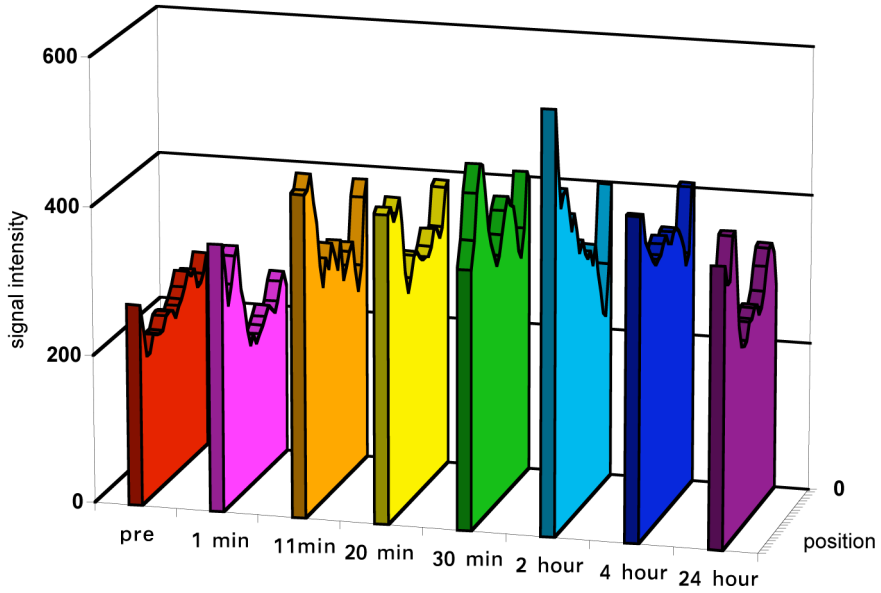

(B)

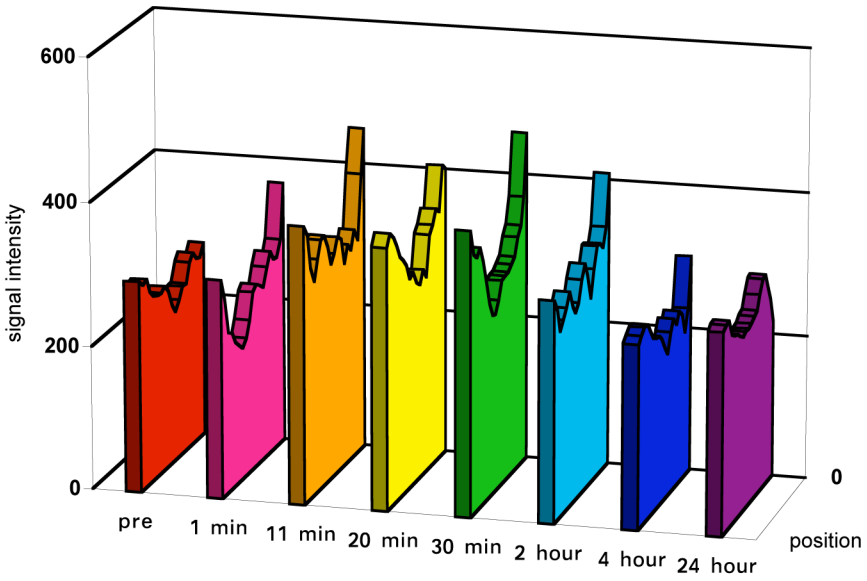

(C)

Figure 4.

Plot profile of signal intensity through tumor tissues before and at various time points after the injection of PGA-1,6-hexanediamine-(Gd-DO3A) conjugates (87 KDa (a), 50 KDa (b), and 28 KDa (c)). The cross section positions are indicated by arrow (4) in Figure 1.

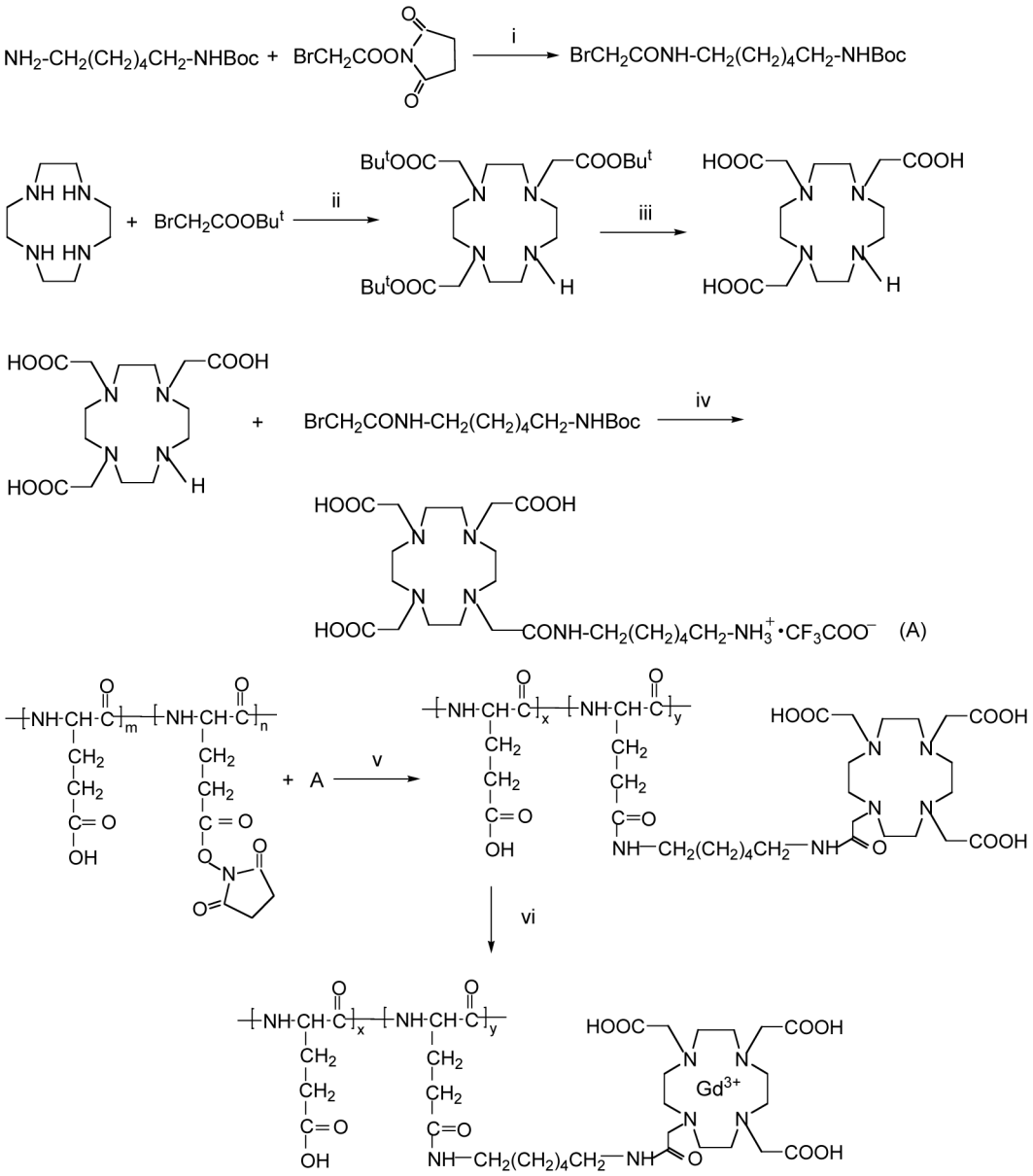

Scheme 1.

Synthetic procedure for PGA-1,6 hexanediamine-(Gd-DO3A). (i) CH_2Cl_2, r.t., overnight; (ii) $CHCl_3$, DIEA, r.t., overnight; (iii) trifluroacetic acid, r.t., 4h; (iv) CH_3OH/triethylamine, K_2CO_3, r.t., overnight, next day trifluroacetic acid, 15 min; (v) DMAP, DMF, r.t., overnight, NaOH; (vi) $Gd(AcO_3)$, Na_2-EDTA, pH 5.0−5.5, r.t., 24h.

Table 1

Physicochemical parameters of PGA-1,6-hexanediamine-(Gd-DO3A).

Fraction number	Molecular weight M_w (KDa)	Molecular weight M_n (KDa)	Gd^{3+} (mol%)	Relaxivity R_1 ($mM^{-1}s^{-1}$)
1	87	60	54.9	9.45
2	74	58	50.2	9.27
3	62	56	38.0	10.47
4	50	45	41.7	9.44
5	44	41	30.4	10.60
6	37	35	40.5	9.66
7	32	29	38.5	9.69
8	28	27	40.2	9.19